Research Article
Open Access
CrossMark

A simulation study of leveling control for railway cranes on curved tracks

Abstract

Compared with ordinary locomotives, railway cranes are characterized by larger load and higher center of gravity. Therefore, leveling control is required in order to ensure safe operation when a railway crane is traveling on a curved track with superelevated outer rail. Accurate simulation of the leveling process requires not only consideration of the influence of wheel-rail motion on curved track, but also reasonable simulation of the lateral and vertical motion of railway crane. A railway crane can be regarded as a complex multi-body system composed of various components. To simulate this system, it is necessary to define rigid and flexible bodies (such as chassis, leveling arc plate, bogie, wheelset and suspension spring), restraints and force elements, and then determine the characteristics of individual components and their connections. In this study, with all the above factors considered, a curved track model was constructed reasonably and then used to simulate the longitudinal kinematic relationship between wheel and rail. Later, a dynamic analysis of the lateral and vertical dynamic responses of railway crane was performed. Moreover, the relationship between the real-time sensor observations and the piston expansion adjustment required was established, and a non-continuous leveling control method was proposed. Based on this, a dynamic simulation software was developed to simulate the mechanical response of railway cranes before and after leveling. This article establishes the relationship between the real-time data obtained by sensors and the expansion and contraction of the leveling cylinder piston. Through calculation, the control data is obtained, which can ensure the smooth operation of the vehicle.

Keywords: railway crane, leveling control, multibody system, wheel-rail motion, curved track

Volume 7 Issue 1 - 2023

Zhao Tianjiao, Qi Zhaohui, Xu jinshuai
Dalian University of Technology, Mechanic Department, Dalian, China

Correspondence: Zhao Tianjiao, Dalian University of Technology, Mechanic Department, Dalian, China, Email tianjiaozha@mail.dlut.edu.cn

Received: August 18, 2023 | **Published:** August 30, 2023

Introduction

In recent years, railway cranes have been widely used for their good operability, high travel speed and superior adaptability. However, when a railway crane operates on a curved track with a heavy load and low speed, the front and rear axle loads are significantly unbalanced, and the component of the car body's gravity directed towards the inner rail is far greater than the required centripetal force. This will cause the crane to tilt overall, making it impossible to ensure its rated lifting performance, safety and reliability, and even causing accidents. Therefore, in order to prevent a reduction in their lifting performance on curves and allow them to pass through curves safely, railway cranes are equipped with an automatic superelevation leveling device, which can keep the chassis levelled when the cranes travel on curves.

Railway cranes are a type of rail vehicle. To explore their leveling control during movement, it is necessary to effectively describe the multi-body system model composed of vehicle components and determine the characteristics of individual components and their connections. Then a series of dynamics equations for the multi-body vehicle system can be obtained and solved.[1] Three common methods for establishing dynamic differential equations are Lagrangian method, Kane method and Newton Euler method.[2–4]

Ling Liang from Southwest Jiaotong University established a longitudinal/transverse/vertical three-dimensional coupling dynamic model for high-speed train based on the rigid multi-body theory and a rigid-flexible coupling dynamic model with a wide analysis frequency range, and studied the dynamic response characteristics of a high-speed train at a variable speed.[5] Based on the theory of flexible multi-body system dynamics combined with the characteristics of vehicle dynamics, Lu Zhenggang established a flexible rigid body dynamics model of railway vehicles for performance prediction, dynamic load calculation and fatigue evaluation, and active vibration control, and carried out research on flexible rigid body dynamics of railway vehicles.[6] Despite abundant research results on railway vehicle dynamics, these is still a lack of simulation work on the automatic leveling system of railway cranes in China. This is because such system is time-varying, nonlinear and easily disturbed, which brings various difficulties to the control process. Chen Zhenhua et al. proposed a control method for automatic leveling of outriggers based on the operation process and safety control requirements for railway cranes.[7] Zhang et al. designed a fuzzy PID controller based on fuzzy logic control algorithm and conventional PID algorithm, combined with the mechanics and mathematical model of the automatic leveling system for railway cranes.[8]

In this paper, a model for the test track was established by deducing the differential equation for transition curves according to the design specification for curved railway tracks. Later, the kinematic relationship between wheel and rail was simulated based on an analysis of the characteristics of wheel-rail contact during movement of a railway vehicle on a curved track. Moreover, based on the principle of virtual power, the connections between components of the railway crane were determined and dynamic equations for the system were set up. A non-continuous automatic leveling control method based on real-time sensor data is presented. Numerical examples demonstrate the correctness of the simulation and the rationality of the proposed method.

Structure and leveling principle of a railway crane

In practical engineering, railway cranes can be divided into many types for different purposes, such as general purpose, construction, rescue, etc., but their structures are basically identical and can be divided into two parts: on-board and off-board parts. The on-board

part is the general term for the upper structures of the crane that can rotate around the revolving center line, including the slewing support and all the structures, mechanisms and systems above it (boom, turntable, driver's cab, machine room, etc.). These are the core parts of a railway crane. "Off-board" part refers to the mechanisms and devices below the slewing support, generally including the traveling mechanism of the crane, train connection devices, leveling devices, chassis, outrigger, etc. The traveling mechanism includes bogie and running drive, which are either dedicated for cranes or common ones in locomotives. The train connection devices are coupler and buffer device, which can be connected to the tractor. A leveling device includes an arc plate, a bi-directional hydraulic cylinder, a supporting slider and other mechanisms installed between the bogie frame and the chassis (Figure 1).[9]

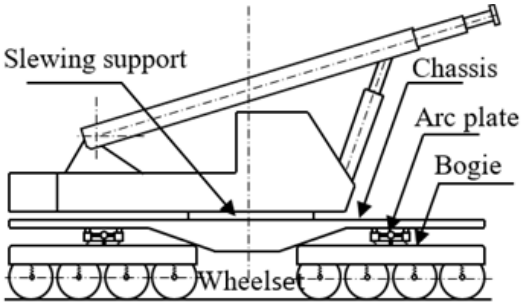

Figure 1 Structural diagram of Railway Crane.

The off-board part of the railway crane includes the components that are most closely related to railway technology, and are also the key components to transfer the external load borne by the on-board part and the entire vehicle's dead weight to the track surface. Therefore, this part plays a very important role in ensuring safety of travelling and lifting. The components of the bogie are connected in a way similar to that in common rail locomotives. The bogie located at the bottom hauls and guides the crane along the rail.[10] It is mainly composed of wheelsets, axle boxes, primary suspension devices, frames, etc. The frame is mounted on wheelsets by primary suspensions to mitigate the impact to the frame caused by track irregularities (Figure 2).

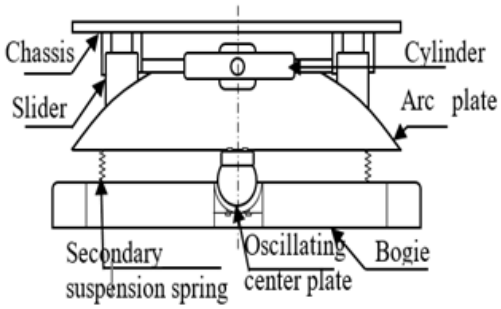

Figure 2 Diagram of leveling device.

Unlike in ordinary locomotives, a leveling device for adjusting the horizontal inclination of a railway crane's chassis is installed between the bogie and the chassis, and it consists of an oscillating center plate, secondary suspension device, arc plate, bi-directional hydraulic cylinder, supporting slider and other components. The arc plate is connected with the bogie through the spherical hinge and can oscillate in all directions, but it is limited by factors like structure size and joint bearing and thus has a maximum swing angle. The secondary suspension device is mainly composed of four steel coil springs with large deflection and rubber pads in series with them, with the left and right sides symmetrically fixed on the bottom surface of the arc plate. One side of each rubber pad contacts the bogie and is allowed to slide on the bogie's top surface so that it can absorb the track impact transferred to the bogie frame again. The bi-directional hydraulic cylinder is connected to the upper part of the arc plate by a pin shaft and rotates around the pin shaft, while its piston is fixed to the chassis. The leveling cylinder and the piston work together. The chassis can be deflected around the arc plate by the supporting slider.

An inclination sensor is installed on the chassis of the railway crane to measure the absolute transverse and longitudinal angles between the chassis and the horizontal plane in real time (the longitudinal direction is along the length of the chassis and the transverse direction is along its width direction). A linkage mechanism is provided between the arc plate's pin shaft and the chassis to measure the relative angle between the longitudinal direction of the arc plate (along its length) and the transverse direction of the chassis in real time. When the crane chassis tilts, it is necessary to determine the adjustment required for piston expansion according to the real-time sensor data. Driven by the bi-directional hydraulic cylinder, the chassis can move inversely around the arc surface of the arc plate installed on the bogie frame to keep the chassis horizontal. In this way, automatic control of railway crane leveling is achieved.

Modeling of curved test track

A curved railway track is generally divided into five parts: straight line, transition curve, circular curve, transition curve and straight line. The transition curve connecting a straight line with a circular curve has a radius of ∞ at the connection with the straight line (straight transition point). As the distance increases, the radius gradually decreases to that of the circular curve, R, at the connection with the circular curve (circular transition point). As the radius decreases, the superelevation increases gradually, and the curves for the purpose of transition are also called easement curves.[11]

At present, the commonly used easement curve on railways is a cubic parabola, which usually can be described by a linear equation:

$$y = \frac{x^3}{6LR} \tag{1}$$

Where R is the radius of the circular curve and L is the length of the parabola. However, the curvature radius of the easement curves at the points where they intersect with the circular curve solved in this way is not equal to the radius of the circular curve, due to some error.

In this paper, given the fact that the radius of the easement curves changes gradually from the straight transition point to the circular transition point, a differential equation for the transition curves is established to overcome the above problems, which is described in detail below.

As shown in Figure 3, a transition curve of length L_0 is inserted between the straight line and the circular curve with radius R, with A denoting the circular transition point and B denoting the straight transition point. Then a coordinate system is established, with the center of the circular curve O taken as the origin point and the angular bisector of the circular curve as the y axis. The negative half of the x-axis is along the tangent to the circular curve at point C, where the circular curve meets its angular bisector. Let P be an arbitrary point on the transition curve, and α be the steering angle or tangent deflection angle (the angle between the tangent at point P and the axis x) with respect to the tangent at point C. The coordinates of point P can be obtained:

$$\begin{cases} x = -\rho \sin \alpha \\ y = \rho \cos \alpha \end{cases} \tag{2}$$

Citation: Tianjiao Z, Zhaohui Q, Jinshuai X. A simulation study of leveling control for railway cranes on curved tracks. *MOJ Civil Eng.* 2023;7(1):28–40. DOI: 10.15406/mojce.2023.07.00170

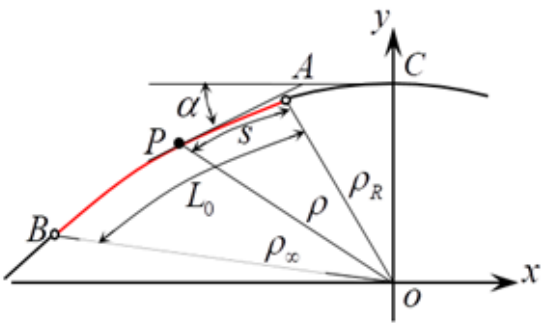

Figure 3 Equation for transition curves.

According to the mathematical definition of curvature, i.e. the rate of change of the forward azimuth angle with the arc length, we can obtain the curvature at point *P*:

$$\kappa_p = \frac{d\alpha}{ds} \tag{3}$$

At the same time, curvature and radius of curvature are reciprocals of each other:

$$\kappa_p = \frac{1}{\rho} \tag{4}$$

According to Formula (2) - (4), the rates of change in *P* point's coordinates with arc length can be obtained:

$$\begin{cases} \dfrac{dx}{ds} = -\cos\alpha \\ \dfrac{dy}{ds} = -\sin\alpha \end{cases} \tag{5}$$

The curvature of the transition curve changes linearly from the circular transition point (curvature $1/R$) to the straight transition point (curvature 0), that is

$$\frac{d\alpha}{ds} = (1 - \frac{s}{L_0})\frac{1}{R} \tag{6}$$

From this, the differential equation for the transition curve can be obtained

$$(\frac{dx}{ds}, \frac{dy}{ds}, \frac{d\alpha}{ds}) = f(x, y, \alpha) \tag{7}$$

The coordinates and steering angle at the circular transition point are selected as the initial values for the equation above:

$$\begin{cases} x_0 = -\rho\sin\alpha_A \\ y_0 = \rho\cos\alpha_A \\ \alpha_0 = \alpha_A \end{cases} \tag{8}$$

An inertial coordinate system $o - xyz$ is created by introducing a *z*-axis to the coordinate system shown in Figure 3 according to the right-hand rule, as shown in Figure 4.[12]

The functional relationship describing the track centerline $\boldsymbol{p}_0 = \boldsymbol{p}_0(s)$ is obtained by solving equation (7). If the base vectors of the inertial coordinate system are $\{\boldsymbol{e}_x, \boldsymbol{e}_y, \boldsymbol{e}_z\}$, the tangent direction of the track centerline is expressed as

$$\boldsymbol{e}_s = \sin\alpha\boldsymbol{e}_x - \cos\alpha\boldsymbol{e}_y \tag{9}$$

And it normal direction is

$$\boldsymbol{e}_n = \cos\alpha\boldsymbol{e}_x + \sin\alpha\boldsymbol{e}_y \tag{10}$$

The function for the inner rail curve corresponding to the arc length coordinate is

$$\boldsymbol{p}_{in} = \boldsymbol{p}_0 - \frac{1}{2}w_0\boldsymbol{e}_n \tag{11}$$

The curve function for the outer rail is

$$\boldsymbol{p}_{out} = \boldsymbol{p}_0 + \frac{1}{2}w_0\boldsymbol{e}_n + z\boldsymbol{e}_z \tag{12}$$

Wherein, $\boldsymbol{w}_0$ is the standard gauge of the track, z is the superelevation value (the height difference between the outer and inner rails), which changes linearly:

$$z=0 \quad s \in \text{Straight line} \tag{13}$$

$$z = z_h \quad s \in \text{Circular curve} \tag{14}$$

$$z = \xi z_h \quad s \in \text{Transition curve} \tag{15}$$

Where, z_h is the superelevation of the circular curve, which ξ varies linearly from 0 to 1.

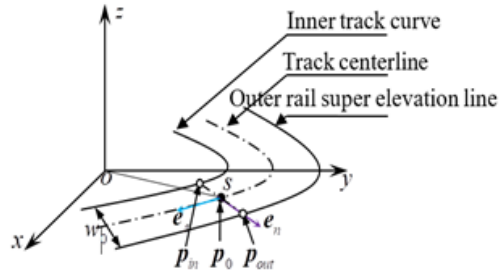

Figure 4 Curve track model.

Kinematic analysis of wheel-rail contact

Wheel-rail relationship is a unique contact relationship in rail vehicles, including railway cranes, and is the basis for simulating the longitudinal motion of railway cranes.[13] Like in other rail vehicles, the wheel treads of railway cranes are mostly rotating conical surfaces. During operation, the lateral relative position between rail surface and tread constantly changes, and slight hunting sometimes occurs. When a crane travels on a curved track, the radius of the rolling circle of a wheel tread contacting the outer rail is greater than that of the corresponding wheel tread contacting the inner rail. This results in a speed difference between the centers of the wheels on the inner and outer rails, thus guiding the crane to turn along the curved track.

In order to simulate and study leveling control for railway cranes and reasonably establish the wheel-rail contact model, this paper primarily considers the influence of curved track's superelevation change and curvature radius change while neglecting the influence of secondary factors such as rail can't change. Additionally, each wheel is treated as a rigid body and given a conical tread.

The number of wheelsets on each bogie of a railway crane varies depending on lifting capacity. This paper takes the common four axle bogie as an example to illustrate. Because the wheelsets are assembled on the bogie frame, the relative position between the wheelsets is constrained by the distance between the centers of axles on the same bogie. Therefore it is reasonable to regard the frontmost wheelset as the driving wheelset first, and derive its wheel-rail contact relationship. The other wheelsets can be regarded as the driven wheelsets and corresponding wheel-rail relationships can be obtained based on relative position constraint.

Citation: Tianjiao Z, Zhaohui Q, Jinshuai X. A simulation study of leveling control for railway cranes on curved tracks. *MOJ Civil Eng.* 2023;7(1):28‒40.
DOI: 10.15406/mojce.2023.07.00170

Spatial description of wheelset attitude

As shown in Figure 5, the arc length coordinates s_1 and s_2 of the contact points between a wheelset and the inner and outer rails, and the sum of the distances d_1 and d_2 between the transient rolling wheel center and the innermost wheel centers are selected as the descriptive variables, so as to uniquely determine the transient state of the contact between the wheelset and the rails.[14]

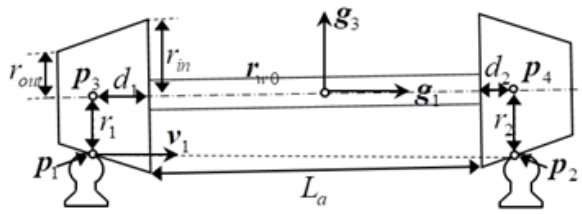

Figure 5 Status of Wheelset on curved track.

Then the radius vectors of the contact points between the wheelset and the inner and outer rails can be expressed as

$$\boldsymbol{p}_1 = \boldsymbol{p}_{in}(s_1) \tag{16}$$

$$\boldsymbol{p}_2 = \boldsymbol{p}_{out}(s_2) \tag{17}$$

The rolling circle radiuses of wheels on the inner and outer rails can be written as

$$r_1 = r_{in} - \delta d_1 \tag{18}$$

$$r_2 = r_{in} - \delta d_2 \tag{19}$$

Wherein, δ is the taper of conical tread and r_{in} is the maximum rolling circle radius of wheel. Rolling centers of wheels on the inner and outer rails are

$$\boldsymbol{p}_3 = \boldsymbol{p}_1 + r_1\boldsymbol{g}_3 \tag{20}$$

$$\boldsymbol{p}_4 = \boldsymbol{p}_2 + r_2\boldsymbol{g}_3 \tag{21}$$

To describe the rotation of the wheelset, two coordinate systems need to be established. One moves together with the wheelset; its origin is at the geometric center of the wheelset, *x*-axis is along the normal direction at the contact point on the inner rail curve, *y*-axis is along the tangent direction at the contact point on the inner rail curve, and the *z*-axis is directed vertically upward. The other is the coordinate system fixed to the wheelset $o - x_w y_w z_w$. The axis x_w points to the outer rail along the direction of the axle, and the axis y_w follows the direction of the wheelset, which conforms to the right-hand rule.

Let $\{\boldsymbol{t}_1, \boldsymbol{t}_2, \boldsymbol{t}_3\}$ be the base vectors of the translational coordinate system $o - xyz$ and $\{\boldsymbol{g}_1, \boldsymbol{g}_2, \boldsymbol{g}_3\}$ be the base vectors of the fixed coordinate system,and then we have

$$\begin{cases} \boldsymbol{t}_1 = \sin\alpha_1\boldsymbol{e}_x - \cos\alpha_1\boldsymbol{e}_y \\ \boldsymbol{t}_2 = \cos\alpha_1\boldsymbol{e}_x + \sin\alpha_1\boldsymbol{e}_y \\ \boldsymbol{t}_3 = \boldsymbol{e}_z \end{cases} \tag{22}$$

Wherein, α_1 is the steering angle corresponding to the arc length coordinate of the inner rail contact point.

The fixed coordinate system is obtained by yawing and rolling the translational coordinate system. In order to facilitate derivation of the steering angle, the rolling angle is divided into two parts. Then the translational coordinate system is rotated three times to obtain the fixed coordinate system. The following transformations are applied to the base vectors: $\{\boldsymbol{t}_1, \boldsymbol{t}_2, \boldsymbol{t}_3\} \to \{\boldsymbol{k}_1, \boldsymbol{k}_2, \boldsymbol{k}_3\} \to \{\boldsymbol{v}_1, \boldsymbol{v}_2, \boldsymbol{v}_3\} \to \{\boldsymbol{g}_1, \boldsymbol{g}_2, \boldsymbol{g}_3\}$

$$\begin{Bmatrix} \boldsymbol{k}_1 \\ \boldsymbol{k}_2 \\ \boldsymbol{k}_3 \end{Bmatrix} = \begin{bmatrix} \cos\vartheta_1 & -\sin\vartheta_1 & 0 \\ \sin\vartheta_1 & \cos\vartheta_1 & 0 \\ 0 & 0 & 1 \end{bmatrix} \begin{Bmatrix} \boldsymbol{t}_1 \\ \boldsymbol{t}_2 \\ \boldsymbol{t}_3 \end{Bmatrix} \tag{23}$$

$$\begin{Bmatrix} \boldsymbol{v}_1 \\ \boldsymbol{v}_2 \\ \boldsymbol{v}_3 \end{Bmatrix} = \begin{bmatrix} \cos\vartheta_2 & 0 & \sin\vartheta_2 \\ 0 & 1 & 0 \\ -\sin\vartheta_2 & 0 & \cos\vartheta_2 \end{bmatrix} \begin{Bmatrix} \boldsymbol{k}_1 \\ \boldsymbol{k}_2 \\ \boldsymbol{k}_3 \end{Bmatrix} \tag{24}$$

$$\begin{Bmatrix} \boldsymbol{g}_1 \\ \boldsymbol{g}_2 \\ \boldsymbol{g}_3 \end{Bmatrix} = \begin{bmatrix} \cos\vartheta_3 & 0 & \sin\vartheta_3 \\ 0 & 1 & 0 \\ -\sin\vartheta_3 & 0 & \cos\vartheta_3 \end{bmatrix} \begin{Bmatrix} \boldsymbol{v}_1 \\ \boldsymbol{v}_2 \\ \boldsymbol{v}_3 \end{Bmatrix} \tag{25}$$

Wherein, ϑ_1 is the yawing angle of the wheelset and $\vartheta_2 + \vartheta_3$ is the rolling angle.

The purpose of the first two rotations is to make the base vector $\boldsymbol{v}_1$ parallel to the line connecting the wheelset's contact points on the inner and outer rails, namely

$$\boldsymbol{v}_1 = (\boldsymbol{p}_2 - \boldsymbol{p}_1)\left\|\boldsymbol{p}_2 - \boldsymbol{p}_1\right\|^{-1} \tag{26}$$

The angles of the first two rotations can be obtained

$$\vartheta_1 = \operatorname{atan}2(-\boldsymbol{v}_1 \cdot \boldsymbol{t}_1, \boldsymbol{v}_1 \cdot \boldsymbol{t}_2) \tag{27}$$

$$\vartheta_2 = \arcsin(\boldsymbol{v}_1 \cdot \boldsymbol{t}_3) \tag{28}$$

The angle of the third rotation can be determined from the rolling circle radiuses of wheels on the inner and outer rails:

$$\vartheta_3 = \arcsin((r_2 - r_1)(L_a + d_1 + d_2)^{-1}) \tag{29}$$

Wherein, L_a is the length of the wheelset axle marked in Figure 5.

Analysis of wheel/rail motion for the driving wheelset

In view of the fact that a railway crane's wheels will neither slip along the track nor rub against rails laterally during normal operation, it is reasonable to assume that the wheel/rail motion is pure rolling without relative sliding in both the longitudinal and transverse directions.

Based on the above pure rolling assumption (no relative sliding between wheel tread and rail), the forward speed of the wheelset is decomposed in the longitudinal and transverse directions of the track. Then it can be inferred that:

1. The speeds of the rolling circle centers of wheels on the inner and outer rails in the forward direction $\boldsymbol{g}_2$ are the product of the angular speed ω of the wheel set and the corresponding rolling circle radius, that is

$$\omega r_1 = \boldsymbol{g}_2 \cdot \dot{\boldsymbol{p}}_3 \tag{30}$$

$$\omega r_2 = \boldsymbol{g}_2 \cdot \dot{\boldsymbol{p}}_4 \tag{31}$$

The forward speed of the crane can be expressed as

$$v_0 = \omega r_1 + (\tfrac{1}{2}L_a + d_1)\boldsymbol{g}_2^T\dot{\boldsymbol{g}}_1 \tag{32}$$

Then the angular velocity of the wheelset can be obtained

$$\omega = r_1^{-1}(v_0 - (\tfrac{1}{2}L_a + d_1)\boldsymbol{g}_2^T\dot{\boldsymbol{g}}_1) \tag{33}$$

Citation: Tianjiao Z, Zhaohui Q, Jinshuai X. A simulation study of leveling control for railway cranes on curved tracks. *MOJ Civil Eng.* 2023;7(1):28–40.
DOI: 10.15406/mojce.2023.07.00170

Equations (30) and (31) can be written as

$$\boldsymbol{g}_2^T \begin{bmatrix} \boldsymbol{p}_{3,1} + r_1\lambda_0\boldsymbol{g}_{1,1} & \boldsymbol{p}_{3,2} + r_1\lambda_0\boldsymbol{g}_{1,2} \\ \boldsymbol{p}_{4,1} + r_2\lambda_0\boldsymbol{g}_{1,1} & \boldsymbol{p}_{4,2} + r_2\lambda_0\boldsymbol{g}_{1,2} \end{bmatrix} \begin{bmatrix} \dot{s}_1 \\ \dot{s}_2 \end{bmatrix} = \begin{bmatrix} \omega_0 r_1 \\ \omega_0 r_2 \end{bmatrix} \tag{34}$$

Where

$$\omega_0 = r_1^{-1} v_0 \tag{35}$$

$$\lambda_0 = r_1^{-1}(\frac{1}{2}L_a + d_1) \tag{36}$$

In which $\boldsymbol{g}_{i,j}$ is $\partial \boldsymbol{g}_i \big/ \partial s_j$ and $\boldsymbol{p}_{i,j}$ is $\partial \boldsymbol{p}_i \big/ \partial s_j$.

2. The components of the rolling center speeds of wheels on the inner and outer rails along the axle direction are

$$\dot{d}_1 = -\boldsymbol{g}_1 \cdot \dot{\boldsymbol{p}}_1 \tag{37}$$

$$\dot{d}_2 = \boldsymbol{g}_1 \cdot \dot{\boldsymbol{p}}_2 \tag{38}$$

3. The above equation can be expressed as

$$\begin{bmatrix} \dot{d}_1 \\ \dot{d}_2 \end{bmatrix} = \boldsymbol{g}_1^T \begin{bmatrix} -\boldsymbol{p}_{1,1} & 0 \\ 0 & \boldsymbol{p}_{2,2} \end{bmatrix} \begin{bmatrix} \dot{s}_1 \\ \dot{s}_2 \end{bmatrix} \tag{39}$$

Equation (34) and Equation (39) together form the first order differential equation for describing the wheelset's motion on the curved track. It can be seen that the motion of the wheelset on the track is determined by the position constraint on the wheelset imposed by the track. Based on this, the kinematic model of the wheel-rail contact is established.

Analysis of the wheel-rail relationship for the driven wheelsets

The bogie and wheelsets are connected by axle boxes equipped with primary suspension devices.[15] While wheelset movement is constrained by the track, the relative position between wheelsets is constrained by the distance between the bogie's wheel centers, In simple terms.

1. The geometric centers of all wheelsets have the same speed along the forward direction $\boldsymbol{g}_2$;
2. The projections of the axles of all wheelsets on the horizontal plane are parallel to each other and their directions are given by

$$\boldsymbol{a}_0 = \boldsymbol{g}_2 \times \boldsymbol{e}_z \tag{40}$$

As shown in Figure 6, the descriptive variable of a driven wheelset can be expressed as

$$s_1 = \rho_1 ; s_2 = \rho_2 \tag{41}$$

$$d_1 = \delta_1 - \frac{1}{2}L_a ; d_2 = \delta_2 - \frac{1}{2}L_a \tag{42}$$

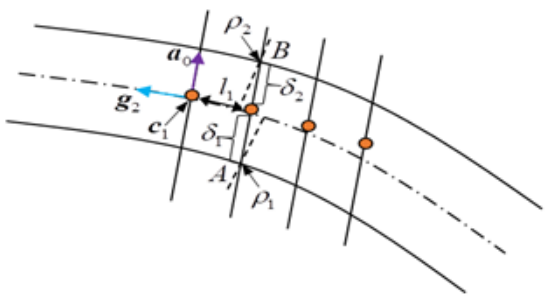

Figure 6 Constraints between wheel sets.

Herein, La is the axle length of the wheelset marked in Figure 5. Calculating the intersection points A and B between the projection of the driven wheel axle on the horizontal plane and the projections of the inner and outer rail curves on the horizontal plane, the nonlinear equations can be derived

$$\begin{cases} \boldsymbol{c}_1 - L_1\boldsymbol{g}_2 + \delta_2\boldsymbol{a}_0 = \left(\boldsymbol{e}_x\boldsymbol{e}_x^T + \boldsymbol{e}_y\boldsymbol{e}_y^T\right)\boldsymbol{p}_{out}\left(\rho_2\right) \\ \boldsymbol{c}_1 - L_1\boldsymbol{g}_2 - \delta_1\boldsymbol{a}_0 = \boldsymbol{p}_{in}\left(\rho_1\right) \end{cases} \tag{43}$$

wherein, $\boldsymbol{c}_1$ is the projection of the radius vector of the driving wheelset's geometric center (the origin of the fixed coordinate system) on the horizontal plane, l_1 is the distance between the centers of the driven and driving wheel axles, $\boldsymbol{p}_{in}(\rho_1)$ and $\boldsymbol{p}_{out}(\rho_2)$ are respectively the radius vectors of contact points between the driven wheels and the inner and outer rails.

Equation (43) is a system of nonlinear equations for calculating the driven wheelset's descriptive variables using known wheel-rail relationship for the driving wheelset, and then determining the wheel-rail relationship for the driven wheelset. In essence, this equation considers not only the constraints between bogie and wheelsets, but also the constraints between track and driven wheelset. Thus it can reflect the actual operation of the crane on the track.

Dynamic analysis of crane in lateral and vertical directions

When simulating and studying the dynamic response of each component of the railway crane during operation, it is necessary to abstract the actual system into a physical or mechanical model, and then establish the corresponding mathematical model, i.e. the differential equation of system dynamics, to find its solution.[16] The chassis (including car body), leveling devices, bogie frame, wheelsets and spring suspension devices of the crane constitute a system composed of springs, dampers and masses.[17,18] However, such a system is a complex multi-body system with multiple degrees of freedom. Studying all of its dynamic characteristics will not only bring great difficulties to analysis and calculation, but also is unnecessary. Therefore, in actual analysis and calculation, the specific objects can be appropriately simplified based on considerations of the main factors affecting the dynamic performance and actual needs, and corresponding assumptions can be made. These assumptions include:

1) Components like wheelsets, bogie frame, leveling arc plates and chassis have much smaller elasticity than the elastic elements of suspension system, and are thus considered as rigid bodies, whose elastic deformation is neglected;
2) Some connections between rigid bodies can be regarded as moving connections formed by proper hinges (spherical hinges, cylindrical hinges, rotary hinges, etc.); The mass of each spring in the suspension device is very small compared with the system mass and is distributed on the rigid body to which it is attached. A spring is regarded as a force element, and only the influence of its elastic deformation on the potential energy of the system is considered;
3) The front and rear bogies have exactly the same structural and size parameters, so do the front and rear leveling devices. The chassis, leveling devices and bogies are symmetrical in structure.
4) Since the pistons in the front and rear leveling devices are firmly connected to the chassis, the oil cylinder is connected to the arc plate by the pin shaft, and each arc plate has four sliders to support the chassis, the chassis, as a whole, restricts the relative position between the front and rear arc plates. The front and rear arc plates have the same orientation during operation.

Citation: Tianjiao Z, Zhaohui Q, Jinshuai X. A simulation study of leveling control for railway cranes on curved tracks. *MOJ Civil Eng.* 2023;7(1):28‒40.
DOI: 10.15406/mojce.2023.07.00170

5) When the railway crane is running, the driving wheels on the front and rear bogies have the same angular velocity around the axle.

Figure 7 shows a simplified topology diagram of the railway crane multi-body system. The wheel-rail relationship essentially describes the longitudinal motion of the crane on the track and it has been obtained in the sections above. On this basis, virtual power equations are derived according to the kinematic relationships between the main components using the virtual power principle, and the dynamic equations for the system are assembled. Then the lateral and vertical dynamic responses of railway crane traveling at different speeds on curved track are calculated.

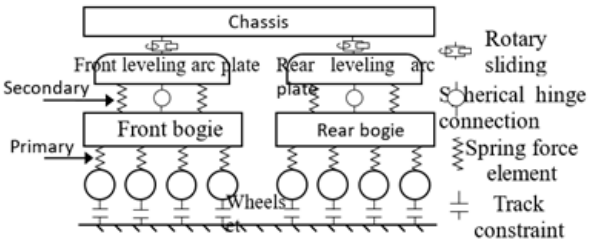

Figure 7 Topology diagram of railway crane multibody system.

Principles of dynamic modeling

The multibody system for a railway crane has multiple spring force elements.[19] The whole system can be regarded as a new particle system composed of the subparticle systems determined by each rigid body. Thus according to the virtual power equation for a single rigid body in a multibody system

$$\delta P_i = \delta \dot{\boldsymbol{r}}_i \cdot \left(m_i \ddot{\boldsymbol{r}}_i - m_i \boldsymbol{g} - \boldsymbol{F}_i^a \right) + \delta \boldsymbol{\omega}_i \cdot \left(\boldsymbol{J}_i \cdot \dot{\boldsymbol{\omega}}_i + \boldsymbol{\omega}_i \times \boldsymbol{J}_i \cdot \boldsymbol{\omega}_i - \boldsymbol{M}_i^a \right) \tag{44}$$

The virtual power equation for a rigid multibody system can be obtained by superposition

$$\delta P_w = \sum_i \delta P_i \tag{45}$$

The force exerted by the spring force elements on the connected object is related to the distance and relative speed between the connection points of the force elements. The relative motion of the object will cause the spring to continuously change in tension and compression, and the potential energy of the suspension devices in the system will change accordingly. The spring can be regarded as a purely flexible element without mass. Its virtual power equation is approximated by the virtual power of flexible body deformation as

$$\delta P_e = \sum_i \delta \dot{\varepsilon}_i f_i \tag{46}$$

In which $f_i = k_i \varepsilon_i$ is the spring force when the amount of deformation is ε_i.

The virtual power equation for the system is

$$\delta P = \delta P_w + \delta P_e \tag{47}$$

Unlike those of a single rigid body, the centroid velocity and angular velocity of each object in a multibody system are not independent. The centroid acceleration of the object can be expressed as $\ddot{\boldsymbol{r}}_i = \boldsymbol{\alpha}_i \ddot{q} + \boldsymbol{w}_i$ and its angular acceleration can be expressed as $\dot{\boldsymbol{u}}_i = \hat{\boldsymbol{a}}_i \ddot{q} + \hat{\boldsymbol{o}}_i$. According to the definition of virtual velocity, the virtual velocity of the object's centroid and the virtual angular velocity of the object are respectively.

$$\begin{cases} \delta \dot{\boldsymbol{r}}_i = \boldsymbol{\alpha}_i \delta \dot{q} \\ \delta \boldsymbol{\omega}_i = \boldsymbol{\beta}_i \delta \dot{q} \end{cases} \tag{48}$$

The virtual variation in the rate of change in the deformation of each spring force element with time is expressed as

$$\delta \dot{\varepsilon}_i = \tilde{\boldsymbol{a}}_i \delta \dot{q} \tag{49}$$

Substituting Eqs. (48) and (49) into Eq. (47), we can get

$$\begin{aligned} \delta P = {} & \delta \dot{q}^T \sum_i \hat{\boldsymbol{a}}_i^T (m_i \hat{\boldsymbol{a}}_i \ddot{q} + m_i \boldsymbol{w}_i - m_i \boldsymbol{g} - F_i^a) \\ & + \delta \dot{q}^T \sum_i \hat{\boldsymbol{a}}_i^T (\boldsymbol{J}_i \hat{\boldsymbol{a}}_i \ddot{q} + \boldsymbol{J}_i \hat{\boldsymbol{o}}_i + \dot{\boldsymbol{u}}_i \times \boldsymbol{J}_i \cdot \dot{\boldsymbol{u}}_i - \boldsymbol{M}_i^a) \\ & + \delta \dot{q}^T \sum_i \tilde{\boldsymbol{a}}_i^T f_i \end{aligned} \tag{50}$$

According to the principle of virtual power $\delta P = 0$, the above equation is further simplified as[20]

$$\delta \dot{q}^T (\boldsymbol{M} \ddot{q} - \boldsymbol{F}) = 0 \tag{51}$$

Since $\dot{q}$ is an independent variable, the dynamic equation for the system can be obtained

$$\boldsymbol{M} \ddot{q} - \boldsymbol{F} = 0 \backslash * \text{ MERGEFORMAT} \tag{52}$$

Rigid body modeling of each part

Rigid bodies in the system include eight wheelsets, front and rear bogie frames, front and rear leveling arc plates, and chassis. Wheelset motion is substituted into the system's equation as a known term. Next, it is necessary to establish a virtual power model for the bogie frames, the arc plates and the chassis successively from bottom to top based on the kinematic relationships between the components.

1) Bogie frame

As shown in Figure 8, a coordinate system $o - xyz$ conforming to the right-hand rule is fixed to the bogie frame, with the spherical center of the spherical bowl where the spherical hinge is installed taken as the origin. The x-axis points towards the outer rail along the lateral direction of the top surface, while the y-axis points towards the forward direction along the longitudinal direction of the top surface. Let $\{\boldsymbol{b}_1, \boldsymbol{b}_2, \boldsymbol{b}_3\}$ be the base vectors of this coordinate system.

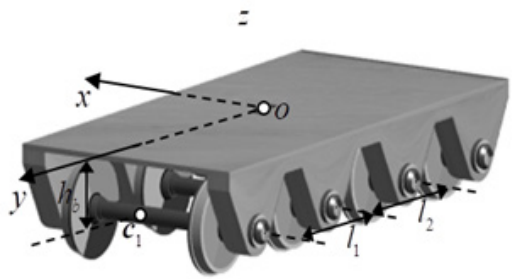

Figure 8 Schematic diagram of the coordinate system fixed to bogie frame.

Taking the coordinate system fixed to the driving wheelset on the bogie frame as the reference system, we mainly consider the effects of the vertical displacement ξ, pitching angle β_1 and rolling angle β_2 of the bogie frame relative to the wheelset caused by the primary suspension device. The relationships between the base vectors can be written as

$$\begin{Bmatrix} \boldsymbol{u}_1 \\ \boldsymbol{u}_2 \\ \boldsymbol{u}_3 \end{Bmatrix} = \begin{bmatrix} \cos\beta_2 & 0 & \sin\beta_2 \\ 0 & 1 & 0 \\ -\sin\beta_2 & 0 & \cos\beta_2 \end{bmatrix} \begin{Bmatrix} \boldsymbol{g}_1 \\ \boldsymbol{g}_2 \\ \boldsymbol{g}_3 \end{Bmatrix} \tag{53}$$

Citation: Tianjiao Z, Zhaohui Q, Jinshuai X. A simulation study of leveling control for railway cranes on curved tracks. *MOJ Civil Eng.* 2023;7(1):28–40.
DOI: 10.15406/mojce.2023.07.00170

$$\begin{Bmatrix} \boldsymbol{b}_1 \\ \boldsymbol{b}_2 \\ \boldsymbol{b}_3 \end{Bmatrix} = \begin{bmatrix} 1 & 0 & 0 \\ 0 & \cos\beta_1 & \sin\beta_1 \\ 0 & -\sin\beta_1 & \cos\beta_1 \end{bmatrix} \begin{Bmatrix} \boldsymbol{u}_1 \\ \boldsymbol{u}_2 \\ \boldsymbol{u}_3 \end{Bmatrix} \tag{54}$$

Then the angular velocity is

$$\boldsymbol{\omega}_b = (\dot{\boldsymbol{b}}_2 \cdot \boldsymbol{b}_3)\boldsymbol{b}_1 + (\dot{\boldsymbol{b}}_3 \cdot \boldsymbol{b}_1)\boldsymbol{b}_2 + (\dot{\boldsymbol{b}}_1 \cdot \boldsymbol{b}_2)\boldsymbol{b}_3 \tag{55}$$

The origin of the coordinate system fixed to the bogie frame, i.e. the center of the spherical hinge, is expressed as

$$\boldsymbol{r}_0^b = \boldsymbol{c}_1 + \xi \boldsymbol{e}_z + h_b \boldsymbol{b}_3 - (l_1 + \frac{1}{2} l_1)\boldsymbol{b}_2 \tag{56}$$

As shown in Figure 8, $\boldsymbol{c}_1$ is the geometric center of the driving wheelset, h_b is the vertical height from the geometric center of the driving wheelset to the origin of the coordinate system fixed to the bogie in the initial state, l_1 and l_2 are the distances between the centers of three adjacent wheel axles. The centroid of bogie frame is

$$\boldsymbol{r}_c^b = \boldsymbol{r}_0^b + \boldsymbol{R}\boldsymbol{p}_b \tag{57}$$

Wherein, $\boldsymbol{R} = [\boldsymbol{b}_1 \quad \boldsymbol{b}_2 \quad \boldsymbol{b}_3]$, and $\boldsymbol{p}_b$ is the component of the bogie frame's centroid in the fixed coordinate system.

The virtual power of the bogie frame relative to the fixed coordinate system can be obtained from equation (44)

$$\delta p_w^b = \delta \begin{bmatrix} \dot{\boldsymbol{r}}_0^b \\ \boldsymbol{\omega}_b \end{bmatrix}^T \left(\boldsymbol{M}_b \begin{bmatrix} \ddot{\boldsymbol{r}}_0^b \\ \dot{\boldsymbol{\omega}}_b \end{bmatrix} + \boldsymbol{F}_b \right) \tag{58}$$

Where the mass matrix

$$\boldsymbol{M}_b = \begin{bmatrix} m_b \boldsymbol{E} & -m_b(\tilde{\boldsymbol{r}}_c^b - \tilde{\boldsymbol{r}}_0^b) \\ m_b(\tilde{\boldsymbol{r}}_c^b - \tilde{\boldsymbol{r}}_0^b) & \boldsymbol{J}_b \end{bmatrix} \tag{59}$$

And the force matrix

$$\boldsymbol{F}_b = \begin{bmatrix} m_b \tilde{\boldsymbol{\omega}}_b \tilde{\boldsymbol{\omega}}_b (\boldsymbol{r}_c^b - \boldsymbol{r}_0^b) - m_b \boldsymbol{g} \\ \tilde{\boldsymbol{\omega}}_b \boldsymbol{J}_b \boldsymbol{\omega}_b + m_b(\tilde{\boldsymbol{r}}_c^b - \tilde{\boldsymbol{r}}_0^b)\boldsymbol{g} \end{bmatrix} \tag{60}$$

In these equations, m_b is the mass of the bogie frame, and $\boldsymbol{J}_b$ is the moment of inertia of the bogie frame relative to the fixed coordinate system.

It is previously assumed that the front and rear bogies have the same composition and symmetrical structure, and the corresponding driving wheels have the same angular velocity around axle during operation. So the rear bogie's frame and wheelsets can be modelled in the same way as those of the front bogie.

2) Leveling arc plate

As the relative position between the front and rear leveling arc plates is constrained by the chassis as a whole, it is reasonable to assume that the front and rear leveling arc plates always have the same orientation during operation, and the line passing through the centers of the front and rear spherical hinges is parallel to the longitudinal direction of the chassis. Otherwise the chassis will be deformed, which is inconsistent with the principles for actual engineering design. This verifies the validity of the previous assumption (Figure 9).

As shown in Figure 10, a coordinate system $o - xyz$ is fixed to a leveling arc plate, with the spherical hinge center being as the origin. The x-axis points to the outer rail along the longitudinal direction (length) of the arc plate, the y-axis points to the forward direction along the transverse direction (width) of the arc plate, and the z-axis points upward along the height of the arc plate. Let $\{\boldsymbol{e}_1, \boldsymbol{e}_2, \boldsymbol{e}_3\}$ represent the base vectors of this coordinate system.

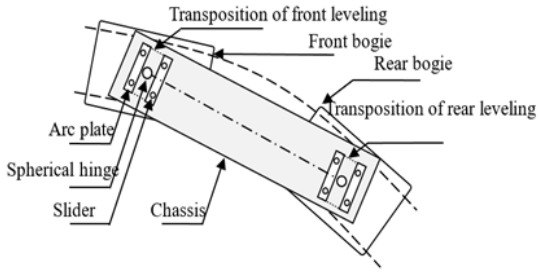

Figure 9 Constraints on front and rear leveling arc plates imposed by chassis.

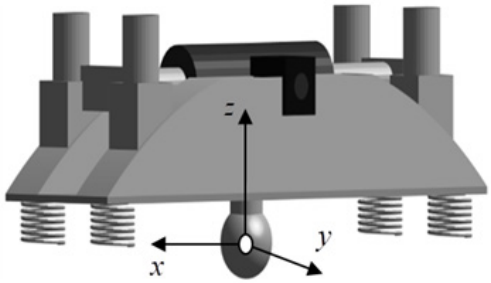

Figure 10 Schematic diagram of the coordinate system fixed to leveling arc plate.

The coordinate system fixed to the bogie frame is used as the reference system. As each leveling arc plate is connected to the bogie frame by a spherical hinge, it is necessary to consider the influence of the yawing angle χ_1, pitching angle χ_2 and rolling angle χ_3 of the leveling arc plate relative to the bogie frame. Thus following transformations are applied to the base vectors:

$$\{\boldsymbol{b}_1, \boldsymbol{b}_2, \boldsymbol{b}_3\} \to \{\boldsymbol{m}_1, \boldsymbol{m}_2, \boldsymbol{m}_3\} \to \{\boldsymbol{n}_1, \boldsymbol{n}_2, \boldsymbol{n}_3\} \to \{\boldsymbol{e}_1, \boldsymbol{e}_2, \boldsymbol{e}_3\}$$

$$\begin{Bmatrix} \boldsymbol{m}_1 \\ \boldsymbol{m}_2 \\ \boldsymbol{m}_3 \end{Bmatrix} = \begin{bmatrix} \cos\chi_1 & \sin\chi_1 & 0 \\ -\sin\chi_1 & \cos\chi_1 & 0 \\ 0 & 0 & 1 \end{bmatrix} \begin{Bmatrix} \boldsymbol{b}_1 \\ \boldsymbol{b}_2 \\ \boldsymbol{b}_3 \end{Bmatrix} \tag{61}$$

$$\begin{Bmatrix} \boldsymbol{n}_1 \\ \boldsymbol{n}_2 \\ \boldsymbol{n}_3 \end{Bmatrix} = \begin{bmatrix} 1 & 0 & 0 \\ 0 & \cos\chi_2 & \sin\chi_2 \\ 0 & -\sin\chi_2 & \cos\chi_2 \end{bmatrix} \begin{Bmatrix} \boldsymbol{m}_1 \\ \boldsymbol{m}_2 \\ \boldsymbol{m}_3 \end{Bmatrix} \tag{62}$$

$$\begin{Bmatrix} \boldsymbol{e}_1 \\ \boldsymbol{e}_2 \\ \boldsymbol{e}_3 \end{Bmatrix} = \begin{bmatrix} \cos\chi_3 & 0 & -\sin\chi_3 \\ 0 & 1 & 0 \\ \sin\chi_3 & 0 & \cos\chi_3 \end{bmatrix} \begin{Bmatrix} \boldsymbol{n}_1 \\ \boldsymbol{n}_2 \\ \boldsymbol{n}_3 \end{Bmatrix} \tag{63}$$

Then the angular velocity is

$$\boldsymbol{\omega}_e = (\dot{\boldsymbol{e}}_2 \cdot \boldsymbol{e}_3)\boldsymbol{e}_1 + (\dot{\boldsymbol{e}}_3 \cdot \boldsymbol{e}_1)\boldsymbol{e}_2 + (\dot{\boldsymbol{e}}_1 \cdot \boldsymbol{e}_2)\boldsymbol{e}_3 \tag{64}$$

The upper surface of each slider on the leveling arc plate forms a plane that coincides with the plane of the chassis. Ignoring the minimal impact of installation clearance on this situation, as shown in Figure 9, the y-axis of coordinate system fixed to the arc plate must be parallel to the longitudinal direction of the chassis, and thereby the line between centers of the front and rear spherical hinges, that is

$$\boldsymbol{e}_2 = \left(\bar{\boldsymbol{r}}_0^e - \bar{\boldsymbol{r}}_0^e\right) \left\| \bar{\boldsymbol{r}}_0^e - \bar{\boldsymbol{r}}_0^e \right\|^{-1} \tag{65}$$

Where $\bar{\boldsymbol{r}}_0^e$ and $\bar{\boldsymbol{r}}_0^e$ are the centers of the spherical hinges on the front and rear leveling arc plates, respectively. They are also the centers of spherical bowls on the front and rear bogie frames for

installting the spherical hinges. Then the yawing angle and pitching angle are respectively

$$\chi_1 = a\tan 2(-\boldsymbol{b}_1 \cdot \boldsymbol{e}_2, \boldsymbol{b}_2 \cdot \boldsymbol{e}_2) \tag{66}$$

$$\chi_2 = a\sin(\boldsymbol{b}_3 \cdot \boldsymbol{e}_2) \tag{67}$$

The centroids of front and rear leveling arc plates are

$$\tilde{\boldsymbol{r}}_c^e = \tilde{\boldsymbol{r}}_0^e + \boldsymbol{R}\boldsymbol{p}_e \tag{68}$$

$$\tilde{\boldsymbol{r}}_c^e = \tilde{\boldsymbol{r}}_0^e + \boldsymbol{R}\boldsymbol{p}_e \tag{69}$$

Where $\boldsymbol{R} = [\boldsymbol{e}_1 \quad \boldsymbol{e}_2 \quad \boldsymbol{e}_3]$ and $\boldsymbol{p}_e$ is the component of the centroid of a leveling arc plate in the fixed coordinate system.

According to formula (44), the virtual power of the front leveling arc plate relative to the coordinate system fixed to it is

$$\delta p_w^e = \delta \begin{bmatrix} \dot{\boldsymbol{r}}_0^e \\ \boldsymbol{\omega}_e \end{bmatrix}^T \left(\boldsymbol{M}_e \begin{bmatrix} \ddot{\boldsymbol{r}}_0^e \\ \dot{\boldsymbol{\omega}}_e \end{bmatrix} + \boldsymbol{F}_e \right) \tag{70}$$

Where, the mass matrix $\boldsymbol{M}_e = \begin{bmatrix} m_e\boldsymbol{E} & -m_e(\tilde{\boldsymbol{r}}_c^e - \tilde{\boldsymbol{r}}_0^e) \\ m_e(\tilde{\boldsymbol{r}}_c^e - \tilde{\boldsymbol{r}}_0^b) & \boldsymbol{J}_e \end{bmatrix}$ (71)

And the force matrix

$$\boldsymbol{F}_e = \begin{bmatrix} m_e\tilde{\boldsymbol{\omega}}_e\tilde{\boldsymbol{\omega}}_e(\boldsymbol{r}_c^e - \boldsymbol{r}_0^e) - m_e\boldsymbol{g} \\ \tilde{\boldsymbol{\omega}}_e\boldsymbol{J}_e\boldsymbol{\omega}_e + m_e(\tilde{\boldsymbol{r}}_c^e - \tilde{\boldsymbol{r}}_0^e)\boldsymbol{g} \end{bmatrix} \tag{72}$$

wherein, m_e is the mass of the leveling arc plate, and $\boldsymbol{J}_e$ is the moment of inertia of the leveling arc plate relative to the fixed coordinate system.

The virtual power of the rear leveling arc plate relative to the coordinate system fixed to it can be obtained in the same way as that of the front leveling arc plate.

1) Chassis (including car body)

As shown in Figure 11, a coordinate system $o - xyz$ conforming to the right-hand rule is fixed to the chassis, with the geometric center of the upper surface of the chassis used as the origin. The x-axis points to the outer rail along the transverse direction (width) of the chassis, and the y-axis points to the forward direction along the longitudinal direction (length) of the chassis. Let $\{\boldsymbol{h}_1, \boldsymbol{h}_2, \boldsymbol{h}_3\}$ be the coordinate system's base vectors.

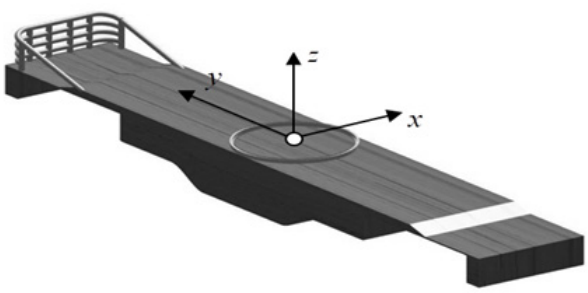

Figure 11 Schematic diagram of the coordinate system fixed to the chassis (including car body).

The coordinate system fixed to a leveling arc plate is used as the reference system.[20–25] According to the constraint on the leveling arc plate imposed by the chassis, the y-axis of the coordinate system fixed to the arc plate is parallel to the y-axis y of the coordinate system fixed to the chassis. Then the movement of the chassis with respect to the leveling arc plate is pure rotation around the base vector $\boldsymbol{e}_2$ (rolling). This relative movement is the result of the joint action of the oil cylinder and piston installed on the leveling arc plate. The model for this relative motion can be simplified as shown in Figure 12.

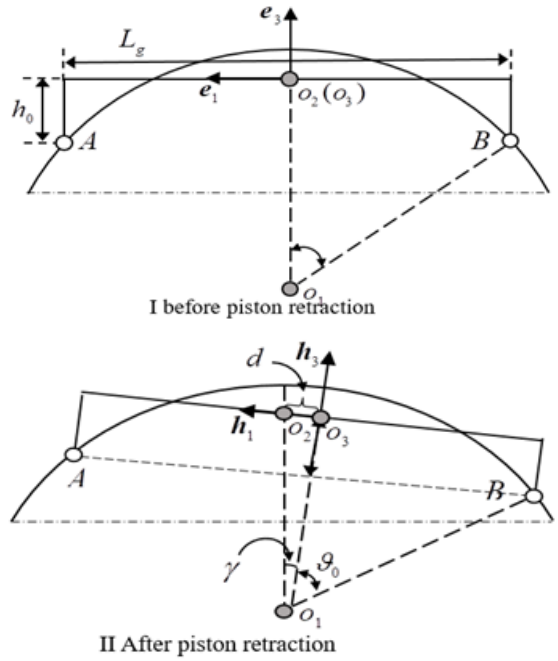

Figure 12 Geometric relation representing the relative motion between chassis and arc plate.

o_1 - Circle center of arc plate; o_2 - Center of pin shaft; o_3 - Piston center

The vertical median lines of the left and right support sliders.

When the leveling cylinder piston is not retracted, the chassis can be regarded as firmly connected with the front and rear arc plates. Then the base vectors of the chassis-fixed coordinate system have the same directions as those of the leveling arc plate. At this time, the initial angle for a given arc radius of the arc plate is

$$\vartheta_0 = \operatorname{asin}(\tfrac{1}{2} L_g R^{-1}) \tag{73}$$

Where R is the arc radius and L_g is the piston length.

Distance from piston center to circle center of arc plate

$$h_g = R\cos\vartheta_0 + h_0 \tag{74}$$

After the right cylinder is retracted by d, the angle of rotation of the chassis relative to the arc plate is

$$\gamma = \operatorname{asin}(d h_g^{-1}) \tag{75}$$

Then the base vector of the chassis-fixed coordinate system is

$$\begin{Bmatrix} \boldsymbol{h}_1 \\ \boldsymbol{h}_2 \\ \boldsymbol{h}_3 \end{Bmatrix} = \begin{bmatrix} \cos\gamma & 0 & \sin\gamma \\ 0 & 1 & 0 \\ -\sin\gamma & 0 & \cos\gamma \end{bmatrix} \begin{Bmatrix} \boldsymbol{e}_1 \\ \boldsymbol{e}_2 \\ \boldsymbol{e}_3 \end{Bmatrix} \tag{76}$$

The angular velocity is

$$\boldsymbol{\omega}_h = (\dot{\boldsymbol{h}}_2 \cdot \boldsymbol{h}_3)\boldsymbol{h}_1 + (\dot{\boldsymbol{h}}_3 \cdot \boldsymbol{h}_1)\boldsymbol{h}_2 + (\dot{\boldsymbol{h}}_1 \cdot \boldsymbol{h}_2)\boldsymbol{h}_3 \tag{77}$$

The origin of the chassis-fixed coordinate system is

$$\boldsymbol{r}_0^h = \tfrac{1}{2}\left(\bar{\boldsymbol{\rho}} + \bar{\boldsymbol{\rho}} - 2d\boldsymbol{h}_1 + 2h_1\boldsymbol{h}_3\right) \tag{78}$$

Wherein, h_1 is the vertical distance between the piston center and the chassis center in the initial state, and $\tilde{\boldsymbol{n}}_1$ and $\tilde{\boldsymbol{n}}_2$ are the centers of pin shafts on the front and rear leveling arc plates.

Citation: Tianjiao Z, Zhaohui Q, Jinshuai X. A simulation study of leveling control for railway cranes on curved tracks. *MOJ Civil Eng.* 2023;7(1):28–40.
DOI: 10.15406/mojce.2023.07.00170

The centroid of the chassis is

$$\boldsymbol{r}_c^h = \boldsymbol{r}_0^h + \boldsymbol{R}\boldsymbol{p}_h \tag{79}$$

Where $\boldsymbol{R} = [\boldsymbol{h}_1 \quad \boldsymbol{h}_2 \quad \boldsymbol{h}_3]$ and $\boldsymbol{p}_h$ is the component of the chassis's centroid in the fixed coordinate system.

The virtual power of the chassis relative to the fixed coordinate system[26] can be obtained from equation (44)

$$\delta p_w^h = \delta \begin{bmatrix} \dot{\boldsymbol{r}}_0^h \\ \boldsymbol{\omega}_h \end{bmatrix}^T \left(\boldsymbol{M}_h \begin{bmatrix} \ddot{\boldsymbol{r}}_0^h \\ \dot{\boldsymbol{\omega}}_h \end{bmatrix} + \boldsymbol{F}_h \right) \tag{80}$$

Where, the mass matrix $\boldsymbol{M}_h = \begin{bmatrix} m_h \boldsymbol{E} & -m_h(\tilde{\boldsymbol{r}}_c^h - \tilde{\boldsymbol{r}}_0^h) \\ m_h(\tilde{\boldsymbol{r}}_c^h - \tilde{\boldsymbol{r}}_0^h) & \boldsymbol{J}_h \end{bmatrix}$ (81)

And the force matrix

$$\boldsymbol{F}_h = \begin{bmatrix} m_h \tilde{\boldsymbol{\omega}}_h \tilde{\boldsymbol{\omega}}_h (\boldsymbol{r}_c^h - \boldsymbol{r}_0^h) - m_h \boldsymbol{g} \\ \tilde{\boldsymbol{\omega}}_h \boldsymbol{J}_h \boldsymbol{\omega}_h + m_h (\tilde{\boldsymbol{r}}_c^h - \tilde{\boldsymbol{r}}_0^h) \boldsymbol{g} \end{bmatrix} \tag{82}$$

Wherein, m_h is the mass of the chassis and $\boldsymbol{J}_h$ is the moment of inertia of the chassis relative to the fixed coordinate system.

Representation of suspension springs and the limit on the swing angles of spherical hinges

Due to the constraints from the spherical bowls, the swing angles of the spherical hinges between bogies and leveling arc plates cannot exceed 1.5 °. The spherical hinges are considered subjected to the action of springs during the swing process. The spring stiffness is shown in the following Figure 13.

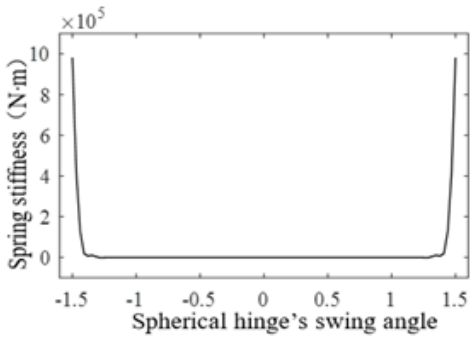

Figure 13 Variation in spring stiffness with spherical hinge's swing angle.

The virtual power equation is

$$\delta P_e = \sum_i \delta \dot{\varepsilon}_i f_i \tag{83}$$

Wherein, the deformation in the suspension spring $\varepsilon_i = \hat{r}_i - \bar{r}_i$ and the deformation in the spherical hinge's spring ε_i is represented by swing angle.

Assembly of dynamic equations for the system

According to the above analysis, the virtual power equation for the system is

$$\delta P = \delta \bar{P}_w^b + \delta \bar{P}_w^b + \delta \bar{P}_w^e + \delta \bar{P}_w^e + \delta P_w^h + \delta P_e^1 + \delta P_e^2 + \delta P_e^c \tag{84}$$

Some parameters can be used as independent parameters to describe the relative motions between components, including vertical displacement ξ, pitching angle β_1 and rolling angle β_2 of front and rear bogie frames relative to their driving wheelsets, the angle between leveling arc plate and the front bogie frame χ_3, and the angle of the chassis relative to leveling arc plate γ. However, γ is determined by the piston of leveling oil cylinder and thus cannot be used as an independent parameter. This will be described in details later in the section about leveling control. Therefore, the array of the selected descriptive parameters is

$$\boldsymbol{q} = [\bar{\xi} \quad \bar{\beta}_1 \quad \bar{\beta}_2 \quad \bar{\xi} \quad \bar{\beta}_1 \quad \bar{\beta}_2 \quad \chi_3] \tag{85}$$

The center acceleration and angular acceleration of each object are

$$\ddot{\bar{\boldsymbol{r}}}_0^b = \bar{\boldsymbol{T}}_0^b \ddot{\boldsymbol{q}} + \bar{\boldsymbol{a}}_0^b ; \dot{\bar{\boldsymbol{\omega}}}_b = \bar{\boldsymbol{T}}_\omega^b \ddot{\boldsymbol{q}} + \bar{\boldsymbol{a}}_\omega^b \tag{86}$$

$$\ddot{\bar{\boldsymbol{r}}}_0^b = \bar{\boldsymbol{T}}_0^b \ddot{\boldsymbol{q}} + \bar{\boldsymbol{a}}_0^b ; \dot{\bar{\boldsymbol{\omega}}}_b = \bar{\boldsymbol{T}}_\omega^b \ddot{\boldsymbol{q}} + \bar{\boldsymbol{a}}_\omega^b \tag{87}$$

$$\ddot{\bar{\boldsymbol{r}}}_0^e = \bar{\boldsymbol{T}}_0^e \ddot{\boldsymbol{q}} + \bar{\boldsymbol{a}}_0^e ; \dot{\bar{\boldsymbol{\omega}}}_e = \bar{\boldsymbol{T}}_\omega^e \ddot{\boldsymbol{q}} + \bar{\boldsymbol{a}}_\omega^e \tag{88}$$

$$\ddot{\bar{\boldsymbol{r}}}_0^e = \bar{\boldsymbol{T}}_0^e \ddot{\boldsymbol{q}} + \bar{\boldsymbol{a}}_0^e ; \dot{\bar{\boldsymbol{\omega}}}_e = \bar{\boldsymbol{T}}_\omega^e \ddot{\boldsymbol{q}} + \bar{\boldsymbol{a}}_\omega^e \tag{89}$$

$$\ddot{\boldsymbol{r}}_0^h = \boldsymbol{T}_0^h \ddot{\boldsymbol{q}} + \boldsymbol{a}_0^h ; \dot{\boldsymbol{\omega}}_h = \boldsymbol{T}_\omega^h \ddot{\boldsymbol{q}} + \boldsymbol{a}_\omega^h \tag{90}$$

The corresponding virtual velocity and virtual angular acceleration are

$$\delta \dot{\bar{\boldsymbol{r}}}_0^b = \bar{\boldsymbol{T}}_0^b \delta \dot{\boldsymbol{q}} ; \delta \bar{\boldsymbol{\omega}}_b = \bar{\boldsymbol{T}}_\omega^b \delta \dot{\boldsymbol{q}} \tag{91}$$

$$\delta \dot{\bar{\boldsymbol{r}}}_0^b = \bar{\boldsymbol{T}}_0^b \delta \dot{\boldsymbol{q}} ; \delta \bar{\boldsymbol{\omega}}_b = \bar{\boldsymbol{T}}_\omega^b \delta \dot{\boldsymbol{q}} \tag{92}$$

$$\delta \dot{\bar{\boldsymbol{r}}}_0^e = \bar{\boldsymbol{T}}_0^e \delta \dot{\boldsymbol{q}} ; \delta \bar{\boldsymbol{\omega}}_e = \bar{\boldsymbol{T}}_\omega^e \delta \dot{\boldsymbol{q}} \tag{93}$$

$$\delta \dot{\bar{\boldsymbol{r}}}_0^e = \bar{\boldsymbol{T}}_0^e \delta \dot{\boldsymbol{q}} ; \delta \bar{\boldsymbol{\omega}}_e = \bar{\boldsymbol{T}}_\omega^e \delta \dot{\boldsymbol{q}} \tag{94}$$

$$\delta \dot{\boldsymbol{r}}_0^h = \boldsymbol{T}_0^h \delta \dot{\boldsymbol{q}} ; \delta \boldsymbol{\omega}_h = \boldsymbol{T}_\omega^h \delta \dot{\boldsymbol{q}} \tag{95}$$

Substituting Eqs. (85) through (94) into Eq. (83) yields

$$\delta \dot{\boldsymbol{q}}^T (\boldsymbol{M}\ddot{\boldsymbol{q}} - \boldsymbol{F}) = 0 \tag{96}$$

Then the dynamic equation for the system is obtained

$$\boldsymbol{M}\ddot{\boldsymbol{q}} - \boldsymbol{F} = 0 \tag{97}$$

Determination of leveling control method for railway cranes

Automatic control systems fall into many categories, and can be divided into continuous control and discontinuous control according to the way of signal collection by sensors. Considering the way of data collection by sensors for railway cranes and the constraints imposed by chassis on the relative position between front and rear leveling arc plates, this paper adopts synchronous leveling of front and rear cylinder pistons and discontinuous automatic control is achieved.

The sensors for railway cranes can actually collect the following data in real time

The angle between the transverse direction $\boldsymbol{h}_1$ of chassis and the absolute horizontal plane

$$\alpha_1 = a\sin(\boldsymbol{e}_z \cdot \boldsymbol{h}_1) \tag{98}$$

The angle between the transverse axis $\boldsymbol{h}_1$ of chassis and the longitudinal direction $\boldsymbol{e}_1$ of arc plate

$$\alpha_2 = a\sin(\boldsymbol{h}_3 \cdot \boldsymbol{e}_1) \tag{99}$$

Set the sampling period t_s and store the sensor data for the three periods between these points: t_0, $t_0 + t_s$, $t_0 + 2t_s$, and $t_0 + 3t_s$. Then the angle values at $t_0 + 4t_s$ can be predicted by polynomial interpolation:

$$\alpha_1\big|_{t_0+4t_s} = -\alpha_1\big|_{t_0} + 4\alpha_1\big|_{t_0+t_s} - 6\alpha_1\big|_{t_0+2t_s} + 4\alpha_1\big|_{t_0+3t_s} \tag{100}$$

Citation: Tianjiao Z, Zhaohui Q, Jinshuai X. A simulation study of leveling control for railway cranes on curved tracks. *MOJ Civil Eng.* 2023;7(1):28–40. DOI: 10.15406/mojce.2023.07.00170

$$\alpha_2\big|_{t_0+4t_s} = -\alpha_2\big|_{t_0} + 4\alpha_2\big|_{t_0+t_s} - 6\alpha_2\big|_{t_0+2t_s} + 4\alpha_2\big|_{t_0+3t_s} \tag{101}$$

According to the geometric relationship shown in Figure 12, the desired value for angle γ at $t_0 + 4t_s$ to keep the chassis levelled is

$$\gamma\big|_{t_0+4t_s} = \alpha_2\big|_{t_0+4t_s} - \alpha_1\big|_{t_0+4t_s} \tag{102}$$

The desired cylinder retraction is

$$d\big|_{t_0+4t_s} = h_g \sin\left(\gamma\big|_{t_0+4t_s}\right) \tag{103}$$

In the interval $\left(t_0 + 3t_s, t_0 + 4t_s\right)$,

$$d = \frac{t_0+4t_s-t}{t_s} d\big|_{t_0+3t_s} + \frac{t-t_0-3t_s}{t_s} d\big|_{t_0+4t_s} \tag{104}$$

$$\dot{d} = t_s^{-1} d\big|_{t_0+4t_s} - t_s^{-1} d\big|_{t_0+3t_s} \tag{105}$$

$$\ddot{d} = 0 \tag{106}$$

According to the formulas, we have

$$\dot{\gamma} = \left(h_g \cos\gamma\right)^{-1} \dot{d} \tag{107}$$

$$\ddot{\gamma} = 0 \tag{108}$$

Therefore, the relationship between the real-time sensor observations and the amount of piston retraction needed to keep the chassis horizontal is established.

The lateral and vertical dynamic equations for railway cranes are a set of differential equations with multiple degrees of freedom. Differential equations can be solved using Newmark method, Wilson θ method, HHT method, generalized α. This paper uses the ODE45 solver, which is a stiff differential equation solver and can ensure the stability of numerical solution.

In order to accurately and effectively simulate the sensors, the data transmitted by the sensors are added to the differential equations as variables to limit the maximum step size, so that simulated sensor data can be obtained and stored in real time based on the time step calculated by the solver. Then the data obtained can be used to accurately and effectively predict the retraction and rotation angle of cylinder for the next time step through polynomial interpolation. The predictions are transmitted to the dynamic equation for the system in real time to simulate the action of actuator in actual operation process.

These are changes that will occur during leveling of a railway crane. When leveling is shut off, the locking cylinder will lock the leveling process. At this time, the retraction of the cylinder is

$$d = 0 \tag{109}$$

And the corresponding rotation angle of rotation is

$$\gamma = 0 \tag{110}$$

These can be substituted into the differential equation to calculate the dynamic response of a railway crane when leveling is shut off.

Numerical examples

Based on the theoretical method presented in this paper, analysis software for use in Matlab environment is developed. It uses ODE45 solver, and its relative accuracy and absolute accuracy are 1e-3 and 1e-4, respectively (Figure 14).

Figure 14 NS1600A Hydraulic railway crane.

Take the size parameters of NS1600A hydraulic railway rescue crane imported from Kirow Leipzig factory in Germany during 2007-2010 as an example to illustrate the calculation results.

First of all, a curved test track model is constructed. Both straight sections are 40m long, and both transition curves have an arc length of 15m. The circular curve has an arc length of 40m, a radius of 240m, and a superelevation of 25mm. The gauge is 1435mm. Using the calculation method for transition curves described in this paper, the variations in the outer rail's curvature and superelevation can be obtained (Figure 15) (Figure 16).

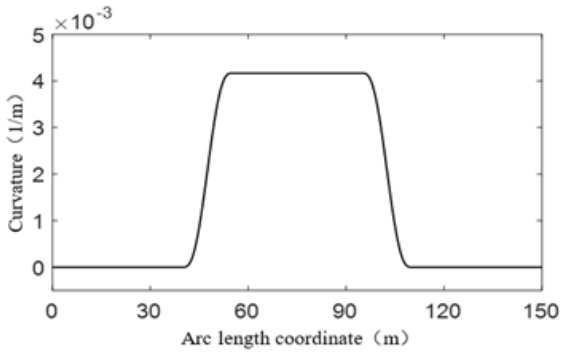

Figure15 Variation in track's curve radius with arc length coordinate.

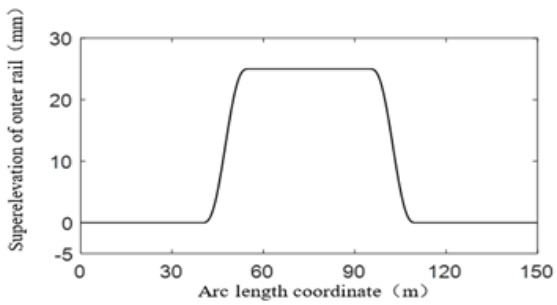

Figure 16 Variation in outer rail superelevation with coordinate arc length.

As shown in the above figure, the transition curves in the railway curve track can be calculated by solving the first-order differential equation. When the length of each section is given, it is possible, in a strict sense, to achieve a gradual curvature increase from 0 to 1/240 and a superelevation increase from 0 to 25 mm, from the straight section to the circular curve. This meets the railway design specifications. Next, let the railway crane carry a load of 64 tons and travel along the curved track model mentioned above at a speed of 40km/h. The responses of each component before and after wheel/

Citation: Tianjiao Z, Zhaohui Q, Jinshuai X. A simulation study of leveling control for railway cranes on curved tracks. *MOJ Civil Eng.* 2023;7(1):28–40.
DOI: 10.15406/mojce.2023.07.00170

rail movement and leveling are calculated. The representation of the involved axles ① - ⑧ is shown in the Figure 17 below.

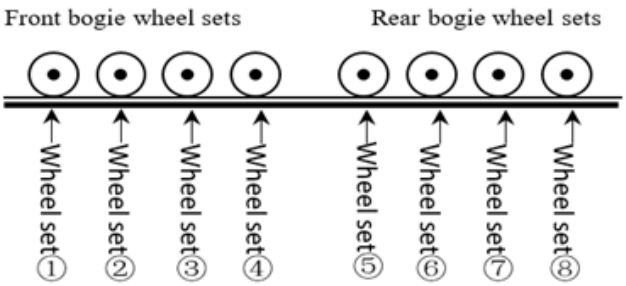

Figure 17 Schematic diagram of numbered wheel sets of the railway crane.

Figure18 shows the lateral displacement of each wheelset of the railway crane along the axle direction during operation. It can be seen that when entering a curved track, each wheel set moves along the axle to the outer edge of the track. As the tread is a rotating conical surface, the rolling radius of the outer rail will be greater than that of the inner rail. This will result in a speed difference between the rolling centers of wheels on the inner and outer rails, leading the crane to turn. It is clear that after the crane moves to the straight section from the curved section, the lateral displacement oscillates, which causes slight hunting of the crane along the track.

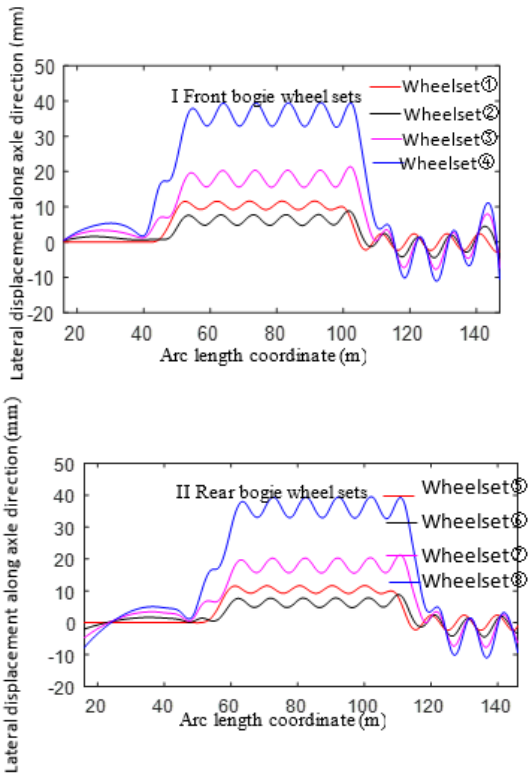

Figure18 Schematic diagram of numbered wheel sets of the railway crane.

Figure 19 shows the arc length coordinate difference between the contact points on the inner and outer rails for each wheelset of the front and rear bogies and reveals the yawing motion of each wheelset on the track. It can be seen from the figure that when the railway crane is traveling on the curved track, the yawing angle of wheelset on each bogie gradually increases, and it will hover slightly at about 0 ° after the crane leaves the curved track.

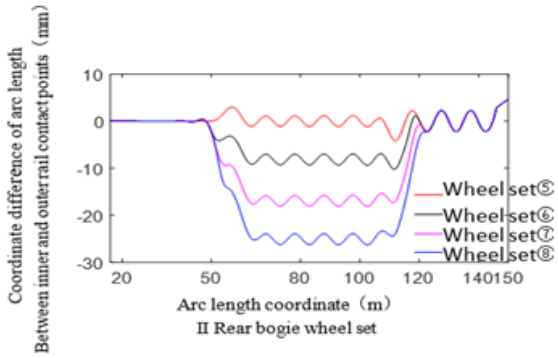

Figure 19 Arc length coordinate difference between inner and outer rail contact points of each wheel set of front and rear bogies.

The sampling period for the simulated sensor is set to 40ms based on the delay time of the hydraulic leveling system of the railway crane. The following figure provides a comparison before and after leveling.

As shown in Figure 20, when the railway crane is traveling with load, its center of gravity will move forward appropriately. As a result, the reaction force applied by the primary spring on the front-bogie wheelset is greater than that on the rear-bogie wheelset. It can be seen from the figure that when the leveling mechanism is turned off, the primary spring's reaction force on the inner driving wheel of the rear bogie will reach -4.42kN, and the absolute value is equal to the gravity of the wheel. At this time, the wheel pressure will be equal to 0. Leveling can help avoid this dangerous situation and greatly reduce the vibration amplitude of the primary suspension spring.

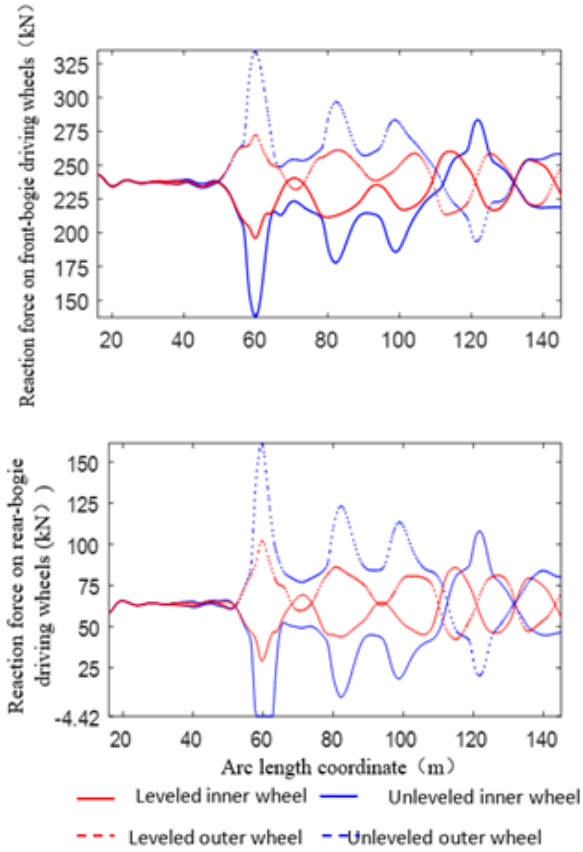

Figure 20 Reaction forces on driving wheels of front and rear bogies exerted by primary suspension springs before and after leveling.

Citation: Tianjiao Z, Zhaohui Q, Jinshuai X. A simulation study of leveling control for railway cranes on curved tracks. *MOJ Civil Eng.* 2023;7(1):28–40.
DOI: 10.15406/mojce.2023.07.00170

As shown in Figure 21, when the railway crane is running on a curved track with leveling disabled, the chassis will incline together with the car body to the outer edge of the track due to centrifugal effect. At the current driving speed, the chassis has a maximum transverse inclination of 6° and tends to swing laterally. After leveling is enabled, the chassis can always be kept horizontal by the leveling cylinder pistons and has a minimal inclination. Figure 22 shows the change in piston retraction during the whole leveling process.

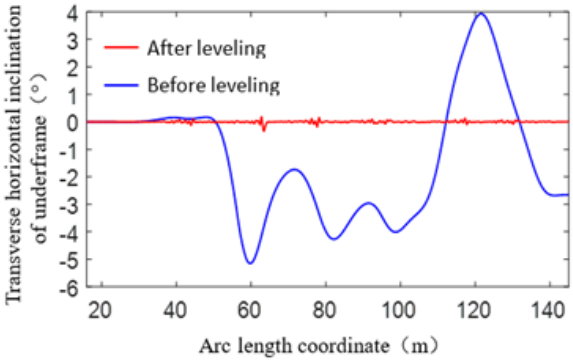

Figure 21 Change of horizontal inclination of underframe before and after leveling.

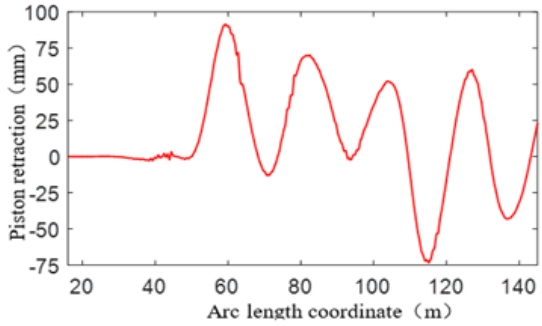

Figure 22 Change in retraction of the cylinder piston during leveling.

In a word, the simulation results from the software developed based on the theoretical method proposed are largely in line with the actual situation of NS1600A hydraulic railway crane traveling on curved track, thus verifying the correctness of the model.

Conclusion

In this paper, longitudinal, transverse and vertical dynamic models were constructed for a railway crane to describe its movement on a curved track. Based on its leveling characteristics, the relationships between real-time sensor data and the retraction of leveling cylinder piston were established by using discontinuous control. The dynamic responses of each component of the railway crane before and after leveling by discontinuous control were simulated and analyzed, and results demonstrate the necessity and effect of leveling. Moreover, analysis software for leveling control of railway cranes was written. It not only can be used to analyze and simulate different types of railway cranes, but also provides a discontinuous control method for synchronous leveling of railway cranes.

Acknowledgments

None.

Conflicts of interests

Author declares there are no conflicts of interests.

Funding

None.

References

1. Bingrong M, Shoune X, Dingchang J. Research on modeling and analysis of a complex multibody system using simpack. *Mechanical Science and Technology for Aerospace Engineering.* 2006;25(7):813–816.
2. Hao Zhu. Research on control strategies for vehicle active suspension based on multi-body dynamics theory. Central South University; 2006.
3. Young TH, Li CY. Vertical vibration analysis of vehicle/imperfect track systems. *Vehicle System Dynamics.* 2003;40(5):329–349.
4. Ripke B, Knothe K. Simulation of high frequency vehicle-track interactions. *Vehicle System Dynamics.* 2007;24(sup1):72–85.
5. Ling Liang. 3D rigid-flexible coupling dynamics of high-speed train/track system. 2015.
6. Lu Zhenggang. Research on dynamic and structural vibration control of flexible rigid body system for railway vehicles. 2005.
7. Zhenhua C, Mingxin T, Cheng N. Design of leveling system for railway rescue crane based on can bus. *Hoisting and Conveying Machinery.* 2012;12:26–29.
8. Zhang L, Shao JP, Sun GT, et al. Research on automatic leveling system of railway rescue crane. *Advanced Materials Research.* 2014;909:241–246.
9. Sisheng F, Liqun Z. Railway rescue cranes. China Railway Publishing House; 2014.
10. Zhou Weijiang. Research on design of signgle-axle driving bogie. Southwest Jiaotong University; 2008.
11. Daoqiu W, Shiming Y, Xiumei Z. Calculation of the cubic parabolic transition curve in high speed railway. Symposium on Traffic Engineering Surveying Technology; 2011.
12. Ping W, Jingmang X, Jiasheng F, et al. Progress in theoretical research on high-speed railway track structure. *High speed railway technology.* 2020;11(2):18–26.
13. Zhang Weihua. Calculation method of wheel/roller (rail) spatial contact point. *Railway Science in China.* 2006;27(4):76–79.
14. Zhaojiu Y, Zhiyuan S, Zhiyuan S, et al. The first monograph on the dynamics of railway large-scale systems in China - review of "vehicle track coupling dynamics". *China Book Review.* 1999;1:58–22.
15. Zhifeng C, Manifesto, Lan W. Research ideas on the dynamics and control of railway vehicle bridge coupling systems. *Science and Technology Innovation Introduction.* 2011;7:253–255.
16. Dalian Y, Hong Z, Bin L. Bogie for CRH2 200km/h EMUs. *Electr Driv Locom.* 2008;3:1–5.
17. Zhang Hui. Study on dynamic performance of high-speed train bogies. Central South University; 2011.
18. Chen Shihua. New development of railway vehicle dynamics simulation. *Railway Vehicles.* 1981;3:6–9.
19. Trees research on the vertical inertia force value of goods under the condition of 27 ton axle load truck. Beijing Jiaotong University. 2017.
20. Qi Zhaohui. Dynamics of multibody systems. Science Press; 2008.
21. Xie Guowei. Simulation of vertical coupling dynamics of railway vehicles and tracks. Kunming University of Science and Technology; 2014.
22. Zhang Jian. Research on optimization design of railway vehicle wheel profile. Southwest Jiaotong University; 2014.

23. Chunshuang N, Qiyong H, Jiazhen H. Overview of multi body dynamics of railway vehicles. *Chinese Railway Science.* 1996;4:1–11.

24. Tianshu W, Caishan L. Progress in multibody dynamics and aerospace dynamics and control. *Journal of Dynamics and Control*. 2018;16(2):95–96.

25. Quan H, Yinghong J, Shijie X. Improvement of Kane's method for multibody system dynamics. *Journal of Mechanics.* 2011;43(5):968–972

26. Zhunyong L, Jiazhen H. Current status and prospects of dynamic research on flexible multi body systems. *Journal of Computational Mechanics.* 2008 ;4:411–416.

Citation: Tianjiao Z, Zhaohui Q, Jinshuai X. A simulation study of leveling control for railway cranes on curved tracks. *MOJ Civil Eng.* 2023;7(1):28–40.
DOI: 10.15406/mojce.2023.07.00170